REPORT DOCUMENTATION PAGE			Form Approved OMB NO. 0704-0188
Public Reporting burden for this collection of information is estimated to average 1 hour per response, including the time for reviewing instructions, searching existing data sources, gathering and maintaining the data needed, and completing and reviewing the collection of information. Send comment regarding this burden estimates or any other aspect of this collection of information, including suggestions for reducing this burden, to Washington Headquarters Services, Directorate for information Operations and Reports, 1215 Jefferson Davis Highway, Suite 1204, Arlington, VA 22202-4302, and to the Office of Management and Budget, Paperwork Reduction Project (0704-0188,) Washington, DC 20503.			
1. AGENCY USE ONLY (Leave Blank)	2. REPORT DATE	3. REPORT TYPE AND DATES COVERED Final Report 10/SEP/02 - 9/SEP/09	
4. TITLE AND SUBTITLE Processing for Highly Efficient A1GaN/GaN UV Emitters		5. FUNDING NUMBERS DAAD190210419	
6. AUTHOR(S) Adesida, Ilesanmi			
7. PERFORMING ORGANIZATION NAME(S) AND ADDRESS(ES) University of Illinois at Urbana-Champaign 1406 West Green St. Urbana IL 61801		8. PERFORMING ORGANIZATION REPORT NUMBER	
9. SPONSORING / MONITORING AGENCY NAME(S) AND ADDRESS(ES) U. S. Army Research Office P.O. Box 12211 Research Triangle Park, NC 27709-2211		10. SPONSORING / MONITORING AGENCY REPORT NUMBER 44421.2-EL-DRP	
11. SUPPLEMENTARY NOTES The views, opinions and/or findings contained in this report are those of the author(s) and should not be construed as an official Department of the Army position, policy or decision, unless so designated by other documentation.			
12 a. DISTRIBUTION / AVAILABILITY STATEMENT Approved for public release: distribution unlimited.		12 b. DISTRIBUTION CODE	
13. ABSTRACT (Maximum 200 words) N A			
14. SUBJECT TERMS		15. NUMBER OF PAGES	
		16. PRICE CODE	
17. SECURITY CLASSIFICATION OR REPORT UNCLASSIFIED	18. SECURITY CLASSIFICATION ON THIS PAGE UNCLASSIFIED	19. SECURITY CLASSIFICATION OF ABSTRACT UNCLASSIFIED	20. LIMITATION OF ABSTRACT U

NSN 7540-01-280-5500

Standard Form 298 (Rev.2-89)
Prescribed by ANSI Std. 239-18
298-102

Enclosure 1

Final Report (2002-2007)

Title: Processing for Highly Efficient AlGaN/GaN emitters

PI Name: Ilesanmi Adesida

Address: University of Illinois
Micro and Nanotechnology Laboratory
208 N. Wright St.
Urbana, Il 61801

Phone Number: 217-333-2150

Fax Number: 217-244-7705

Email Address: iadesida@illinois.edu

Award Number: DAAD19-02-1-0419

Web Site: http://nanoscale.micro.uiuc.edu

Contact: Dr. John Zavada
U.S Army Research Office
ATTN: RDRL-ROE-L
P.O. Box 12211
Research Triangle Park, NC 27709-2211
919.549.4238
john.zavada@aro.army.mil

1. Introduction

The fabrication of high-quality ohmic contacts on *n*- and *p*-type (Al,In)GaN is essential for improving the performance of optoelectronic devices, such as blue light-emitting diodes, metal–semiconductor field effect transistors, HEMTs, and laser diodes. In particular, to realize solid-state UV emitters for chembioagent detection and general lighting, the formation of reliable ohmic contact systems for both *n*- and *p*-AlGaN with relatively high Al contents are indispensable.

In conjunction with efforts to achieve low-resistance ohmic contacts to GaN using low work-function metal contacts, surface treatment techniques have also been proposed as an additional route to improve ohmic contacts, as the nature of the GaN surface is crucial to the formation of high quality ohmic contacts. gallium oxide is formed on GaN and AlGaN surfaces when epilayers are exposed to ambient atmosphere. This native oxide acts as a thin insulating layer over the conducting epilayer. Metal contacts deposited on such semiconductors with surface oxides form a metal-insulator-semiconductor structure instead of a metal-semiconductor junction. Thus, it is imperative to remove the native oxide prior to metal deposition on the semiconductor to form low-resistance ohmic contacts. Apart from the removal of native oxides prior to metallization, plasma treatment techniques have been described for improving ohmic performance of contacts on GaN-based semiconductors. We investigated the effects of $SiCl_4$ plasma treatment and subsequent cleaning in BOE, HCl, and NH_4OH solutions on *n*-GaN and *n*-AlGaN surfaces using XPS and AES. The efficacy of the different surface treatment schemes were compared by monitoring the oxygen concentrations on the surface of the GaN and $Al_xGa_{1-x}N$ materials.

As for ohmic contacts to *n*-AlGaN, Ti- or Ta-based metallization schemes, such as Ti/Al, Ta/Ti/Al, Ti/Ta/Al, and Ti/Al/(Ti, Ni, Mo, and Pt)/Au, have been widely investigated. In such metallization schemes, low specific contact resistivities ranging from $\sim 10^{-5}$ to $\sim 10^{-8}$ Ω-cm^2 have been reported, and these are excellent for the operation of the electronicdevices such as HEMTs and heterojunction bipolar transistors. However, ohmic contact formation to *p*-AlGaN alloys has been difficult to realize. There are two main obstacles to developing device quality ohmic contacts to these materials. The first derives from the difficulty in growing high-quality *p*-AlGaN with high Al contents. The second arises from the absence of metals having a work function larger than that of *p*-AlGaN. For these reasons, only very limited results have been reported so far. In this study several different metal schemes, such as Pt/Pd/Au, Pd/Ni/Au, and Pd/Ir/Au, were investigated to obtain low-resistance ohmic contacts to p-type GaN and AlGaN. The LED heterostructures used consisted of 0.2 μm Mg-doped, *p*-type GaN at the top with subsequent layers of 50 nm InGaN quantum well, 3 μm Si-doped *n*-type GaN on the GaN buffer layer grown on a sapphire substrate were fabricated and characterized, in which Pd/Ir/Au was used as the *p*-contact metallization.

2. Investigation of Surface Treatment for Excellent Ohmic Contact Formation

The following samples were prepared for XPS measurements. Sample 1 was the as-grown GaN layer without any surface treatment while sample 2 was treated with $SiCl_4$ plasma in a reactive ion etching (RIE) system with a plasma self-bias voltage of −300 V for 60 s. Samples 3, 4, and 5 were treated with $SiCl_4$ plasma and followed by a 2-min dip in NH_4OH, HCl, and BOE solutions, respectively.

XPS spectra of Ga3*d* photoelectrons, deconvoluted into Ga–O and Ga–N components, for the various samples are shown in Fig. 1. The Ga3*d* peaks exhibited a blueshift of about 0.2 eV toward the higher binding energy in the samples treated with

$SiCl_4$ plasma and chemically etched. This suggests that the Fermi level (E_F) at the surface of the GaN moved near the conduction band edge due to the plasma and wet etching treatments, resulting in the thinning of effective Schottky barrier height (SBH) for electron transport. This type of shift is believed to be caused by the loss of N at the surface, creating N vacancies, which would increase the *n*-type doping at the surface. The XPS spectra of the N1*s* photoelectrons are shown in Fig. 2. The N1*s* peaks also display a shift of 0.23 eV toward the higher binding energy as similarly obtained for the Ga3*d* photoelectron XPS spectra. However, minimal reduction in the intensity of the N1*s* spectra, which were normalized with Ga3*d* peak areas of the respective samples, for the plasma-treated samples is observed.

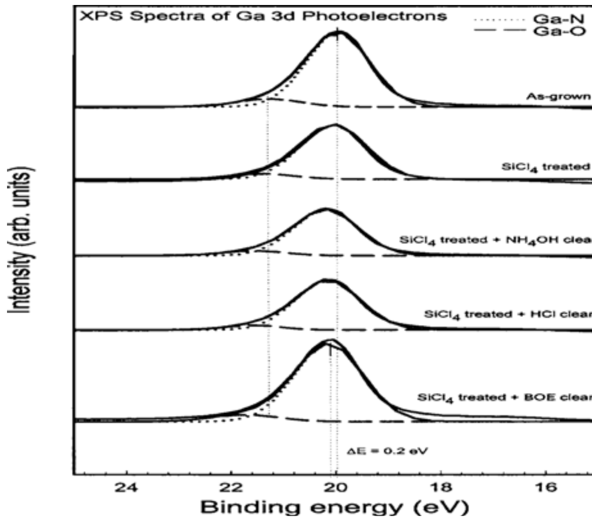

FIG. 1. XPS spectra of Ga3*d* photoelectrons for GaN as a function of surface treatment condition.

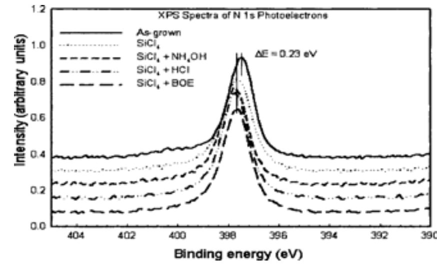

FIG. 2. XPS spectra of the N1*s* photoelectrons for the GaN surface treated under the several conditions.

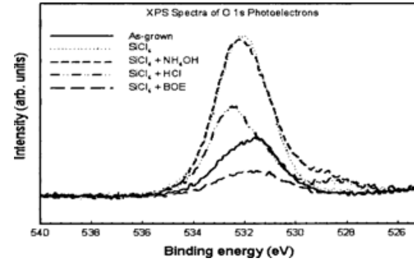

FIG. 3. XPS spectra of the O1*s* photoelectrons for the GaN surface treated under several

The O1*s* photoelectron XPS spectra, shown in Fig. 3, exhibit the oxygen concentration on the surface of GaN after the surface treatment. It is noted that the oxide concentration increased on the surface of the sample treated with $SiCl_4$ plasma compared with that on the as-grown sample. This suggests that the plasma-treated sample had an increased tendency to oxidize since the stoichiometry of the GaN on the surface had been altered. This can be attributed to the evolution of N during the $SiCl_4$ RIE plasma treatment and reaction with O and Ga atoms to form oxynitrides during exposure to ambient atmosphere. It is also seen from Fig. 3 that BOE treatment is the most effective in removing the oxide from the surface of GaN when compared to NH_4OH and HCl treatments. The deconvolution of the spectra into Ga–N and Ga–O bonding components can elucidate the nature of bonding state of Ga atoms on the surface. In this case, Fig. 4. shows the summary of ratio of O/N peak areas; such deconvolution shows that BOE nearly eliminates the Ga–O component. The shifts in the binding energy of the O1*s* spectra and overall peak broadening were attributed to Ga_2O_3 and oxynitrides in GaN surface oxide. A comparison of the N to O ratio within each

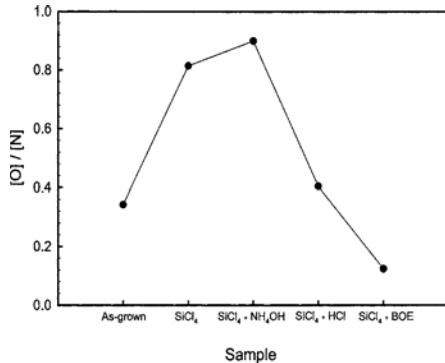

Fig.4. Summary of ratio of O/N peak areas

sample is utilized to gain understanding of the evolution of the surface stoichiometry as a result of the different surface treatment schemes. As discussed above, the small binding energy shift to be in the XPS peaks, which is indicative of a shift of the E_F toward the conduction band, is believed to be due to loss of N from the surface. The value of the O:N ratios can increase due to both an increase in O concentration and/or a decrease in N at the surface. For the purposes of this discussion, the change in O concentration is believed to be greater than the decrease in N concentration and the relative ratios are valid. The ratios of the areas of O1s/N1s peaks for all the samples are summarized in Fig. 4. The O/N ratio for the $SiCl_4$ plasma-treated sample is higher compared to that of the as-grown sample, indicating an increase in the surface oxide concentration relative to N. The sample treated in $SiCl_4$ plasma plus NH_4OH etch exhibits a slight increase in the O/N ratio and this suggests that the NH_4OH solution facilitates the oxidation of the surface instead of the removal of the native oxide. The O/N ratio for the $SiCl_4$ plasma treated plus HCl etched is lower than that of the sample treated with $SiCl_4$ plasma only, but the sample treated in $SiCl_4$ plasma plus BOE has the smallest of the O/N ratio.

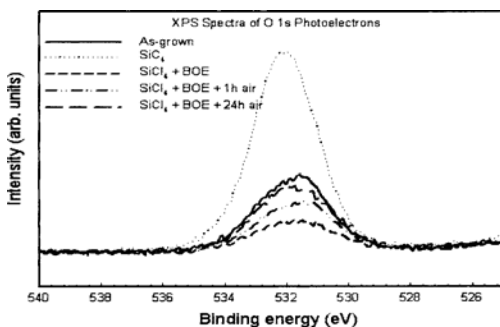

FIG. 5. XPS spectra of the O1*s* photoelectrons for the GaN surface treated with BOE and then exposed to air for various intervals of time.

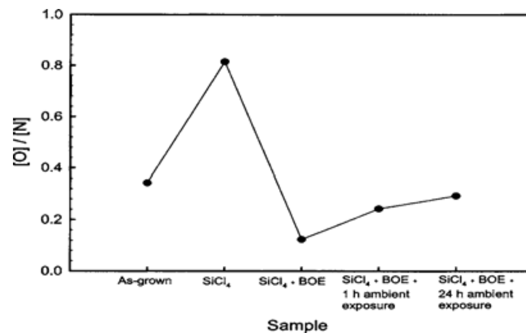

FIG. 6. Summary of ratio of O/N peak areas in the GaN samples treated in BOE and exposed to air for various intervals of time.

The rate of oxidation on a GaN sample that was $SiCl_4$ plasma treated and BOE cleaned was investigated. For this study, the following samples were prepared: as-grown, $SiCl_4$ plasma treated, $SiCl_4$ plasma treated, and BOE cleaned. Of the plasma treated and BOE cleaned samples, the two were exposed to ambient atmosphere after surface cleaning in BOE for 1 and 24 h, respectively. XPS spectra of the O1*s* photoelectrons for the various samples are shown in Fig. 5, and the O/N ratios are summarized in Fig. 6.

From Figs. 5 and 6, it is seen that oxygen concentration on the surface of the treated GaN increased after exposure to ambient atmosphere, as it is evident from the increase in intensity of the O1*s* peak, which were normalized with the Ga3*d* peak areas for the respective samples, and the O/N ratio. However, the increase is not significant compared to the plasma-treated samples, since the O/N ratio of Sample 5, which was exposed to atmosphere for 24 h, is 0.2 while that of Sample 2, which was treated with $SiCl_4$ plasma, is 0.81, and that of Sample 3, which was treated with $SiCl_4$ plasma and cleaned in BOE, is 0.12. After 24 h of exposure, however, the amount of oxide on the surface reaches a level, which is comparable to that of the as-grown sample. Hence, it can be concluded that the rate of oxidation in ambient atmosphere on the surface of GaN after cleaning with BOE is rather insignificant in comparison to the level of oxide concentration on the plasma treated samples. This result demonstrates the effectiveness of this procedure at removing the oxide and keeping it off for enough time to send the wafer to the next processing step-metal deposition.

XPS measurements were also performed to study the effects of surface treatments on AlGaN samples. The as-grown sample (1), and $SiCl_4$ plasma-treated samples (2,3,4,5)

were analyzed for surface stoichiometry with high-resolution XPS. Samples 3, 4, and 5 were further cleaned in NH_4OH, HCl, and BOE solutions for 2 min, respectively, and also analyzed with XPS for surface stoichiometries. XPS spectra of the Ga3*d* photoelectrons for the various samples are shown in Fig. 7. The Ga3*d* peaks of the Ga–N component exhibit a shift of about 0.25 eV toward the higher binding energy in the samples treated with $SiCl_4$ plasma. The shift for the sample that was only plasma-treated is contrary to what was observed in the case of GaN. The XPS spectra of the O1*s* photoelectrons, normalized with respective Ga3*d* peak area for each sample, for the as-grown and various surface-treated samples are shown in Fig. 8. O/N ratios for the AlGaN surface treated samples are summarized in Fig. 9.

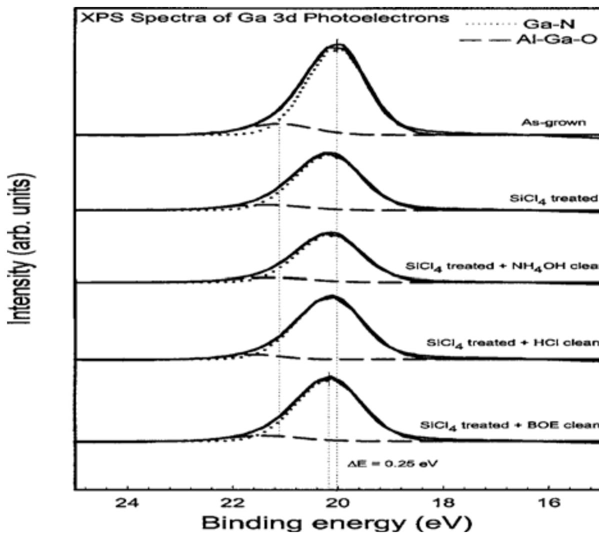

FIG. 7. XPS spectra of the Ga3*d* photoelectrons for the Al0.20Ga0.80N surface treated under several conditions.

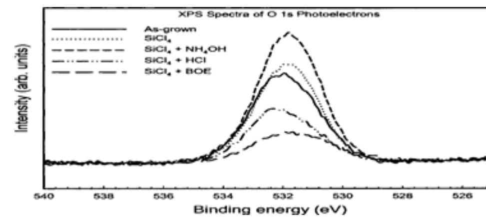

FIG. 8. XPS spectra of the O1*s* photoelectrons for the AlGaN surface treated under several conditions

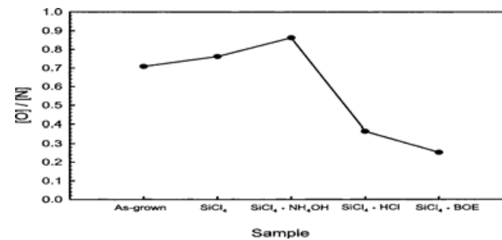

FIG. 9. Summary of ratio of O/N peak areas in the AlGaN samples

The O1*s* peak magnitude for the $SiCl_4$ plasma-treated sample and the NH_4OH cleaned sample are larger than those in the as-grown sample indicating that the $SiCl_4$ plasma treatment alters the surface stoichiometry of the samples. The increase in surface oxide concentration is attributed to the evolution of N during $SiCl_4$ plasma treatment and the subsequent oxidation of the surface in ambient atmosphere. The O/N ratio for the $SiCl_4$ plasma treated sample is larger than that for the as-grown sample, and this corroborates the increase in surface oxide and the decrease in N concentration on the surface of AlGaN with plasma exposure. The samples treated with HCl and BOE exhibit lower surface oxide concentration compared to the as-grown sample as indicated by the O/N ratios for these samples. Both the O/N ratio (and the intensity of the O1*s* peak) are the smallest for the samples, which was cleaned in BOE. From this result, we conclude that BOE is the most effective treatment to remove surface oxides on AlGaN when compared with HCl and NH_4OH treatments. We have also investigated AlGaN samples treated with $SiCl_4$ plasma, cleaned in BOE for 2 min and exposed to ambient atmosphere for 1 and 12 h, respectively, prior to XPS characterization.

In Figs. 10 and 11, XPS spectra of the O1*s* photoelectrons and O/N ratio for the as-grown AlGaN, $SiCl_4$-plasma-treated samples, and the sample treated with $SiCl_4$ plasma and cleaned in BOE and those exposed to air for 1 and for 12 h, respectively, after plasma treatment and surface cleaning in BOE are shown. From the XPS measurements, we can observe that the rate of oxide re-growth on AlGaN samples treated with BOE is insignificant even after 12 h of exposure to ambient atmosphere. This is a slower

oxidation rate that what was observed for GaN, and it is good for processing of AlGaN-based devices. Among the issues of concern with $SiCl_4$ plasma treatment is whether Si atoms are deposited on the surface of $Al_xGa_{1-x}N$. It is of interest to identify what role such deposited atoms play on ohmic contact formation, as Si atoms could act as *n*-type dopant. For this purpose, AES survey scans of as-grown AlGaN and $SiCl_4$-plasma-treated AlGaN samples were taken. A survey scan is presented in Fig. 12 in which Sample 1 is the as-grown AlGaN epilayer, while samples 2–6 have been treated with $SiCl_4$ plasma for 60 s at −50, −100, −200, −300, and −400 V, respectively. Al, Ga, N, O, C, and Si peaks are identified in the AES surface scans. As shown in Fig. 12, $SiCl_4$ plasma treatment causes deposition of Si on the AlGaN surface. The intensity of Si peaks increases slightly with the plasma bias voltage. Also the ratio of intensities of O to N peaks increases with an increase in $SiCl_4$ plasma bias voltage when compared with the AES scan of the as-grown sample. This suggests an increase in N loss with an increase in $SiCl_4$ plasma bias voltage. AES surface scans of AlGaN as-grown and surface treated samples are shown in Fig. 12. Sample 1 is the as-grown AlGaN epilayer, while samples 2–6 have been treated with $SiCl_4$ plasma at −300 V. Samples 3, 4, and 5 were cleaned in NH_4OH, HCl, and BOE for 2 min. After cleaning the surface in BOE, sample 6 was further exposed to ambient atmosphere for 12 h. From the figure, it is noted that in sample 2, $SiCl_4$ plasma treatment causes the deposition of Si on the AlGaN surface and also results in a ratio of O/N peak intensities that is more than that of the as-grown sample. Cleaning the samples in NH_4OH does not decrease the O peak intensity.

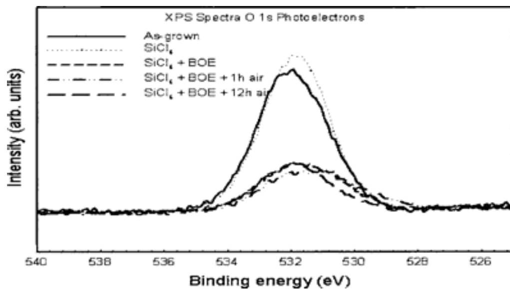

FIG. 10. XPS spectra of the O1*s* photoelectrons for the AlGaN surface treated with BOE and then exposed to air for various intervals of time.

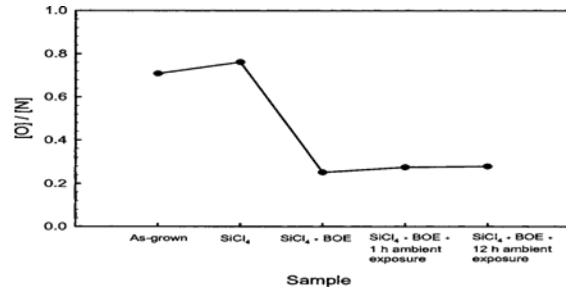

FIG. 11. Summary of ratio of O/N peak areas in the AlGaN samples treated in BOE and exposed to air for various intervals of time.

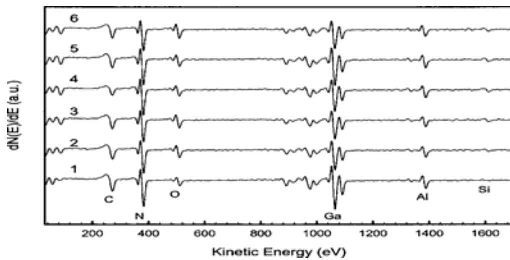

FIG. 12. AES surface scans of as-grown AlGaN sample 1 and those surfaces treated with $SiCl_4$ plasma at different plasma bias voltages, −50 V , −100 V , −200 V , −300 V , and −400 V .

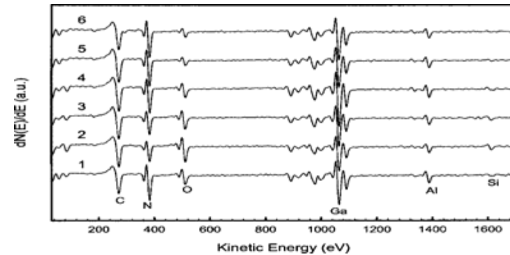

FIG. 13. AES surface scans of as-grown AlGaN sample and those surface treated with $SiCl_4$ plasma at −300 V plasma bias voltage and then cleaned in NH_4OH , HCl , BOE.

However, treating the samples in HCl and BOE does reduce the O peak intensity with BOE being the most efficient etchant for oxide removal. With exposure to air for 12 h after BOE surface treatment, there is a slight increase in oxide concentration on the surface of the sample suggesting reoxidation of the surface after surface treatment much as observed with XPS. As shown in Fig. 13, cleaning the sample in BOE eliminates the Si peak. The elimination implies that the Si may have existed as SiO_x due to ambient oxidation since BOE treatment was very effective in removing Si–O species. It also shows that the Si deposited during the $SiCl_4$ treatment does not play an active role in the improvement of ohmic contact formation.

3. Investigations of low resistance ohmic contacts to p-type GaN and AlGaN

3.A Low-resistance Pt/Pd/Au ohmic contacts to p-type GaN

Figure 14 shows typical *I –V* characteristics of Pt/Pd/Au contacts on *p*-AlGaN as a function of annealing temperature, measured between pads with a spacing of 3 μm. The as-deposited sample exhibited a rectifying *I–V* characteristic due to the large work function of *p*-AlGaN. However, the *I–V* behavior became increasingly linear as the annealing temperature increased. The sample annealed at 600 °C shows a linear *I –V* characteristic, indicating the formation of ohmic contact. The contact resistance (R_c) and the sheetresistance (R_s) were determined from the intercept of the *y* axis and the slope of total resistance (R_T) versus pad spacing. Specific contact resistivity was calculated by $\rho_c = R_c^2/R_s$. Measurement showed that the contact resistivity of the 600 °C-annealed sample was 3.1 x 10^{-4} Ω-cm^2. The contact, however, became degraded when annealed at temperatures in excess of 600 °C, showing that the optimum anneal temperature was 600 °C. The electrical degradation of the samples annealed above 600 °C could be due to severe interfacial reactions and surface degradation.

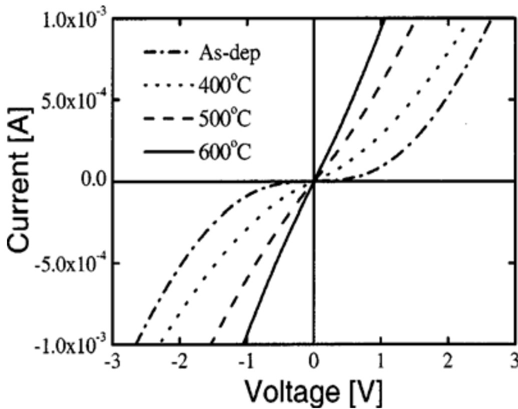

FIG. 14. *I –V* characteristics for the Pt/Pd/Au contacts on *p*-AlGaN as a function of annealing temperature.

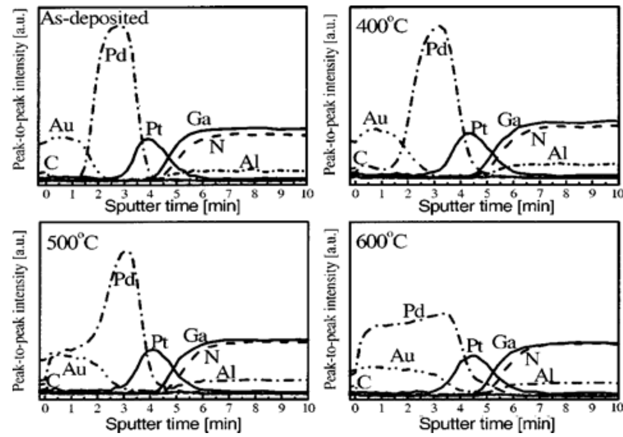

FIG. 15. Auger depth profiles for (a!)the as-deposited, (b) 400 °C, (c) 500 °C, and (d) 600 °C annealed samples.

Figure 15 shows AES depth profiles for the Pt/Pd/Au contacts on the AlGaN as a function of annealing temperature. For the as-deposited sample in Fig. 15(a), each layer is well defined and there is no obvious indication of inter-diffusion between the metal layers and the AlGaN. For the sample annealed at 400 °C, Fig. 15(b), some amount of Pd out-diffused to the surface of the sample through the Au layer and also diffused into the Pt layer. However, there is no evidence for the out-diffusion of both nitrogen and Al into the metal layer. For the 500 °C sample in Fig. 15(c), more Pd out-diffused to the sample surface, which may participate in the formation of a Pd–Au alloy. In addition, a small amount of Pd diffused into the interface region. For the 600 °C sample [Fig. 15(d)], it can be seen that a small amount of Pd and Pt diffused into the AlGaN, as confirmed by the Auger spectral data (Fig. 16). Both the Pd and Pt Auger electron peaks were detected at the interface region between the metal and the AlGaN. This indicates possible reactions between Pt and Pd, and Ga, resulting in the formation of interfacial gallide phases.

To characterize the chemical bonding states of Ga, XPS examination was made of the Pt/Pd/Au contacts on *p*-AlGaN before and after annealing at 600 °C. Figure 17 shows the Ga2*p* core-level spectra obtained from the metals/AlGaN interface regions of the samples. It is clearly shown that the Ga2*p* core level from the interface region of the annealed sample shifts toward the low-binding energy side, compared to that from the as-deposited sample. In other words, the Ga2*p* core level of the interface experienced a shift of about 0.6 eV, compared to that of the as-deposited one. This indicates that annealing

causes the surface Fermi level to shift toward the valence-band edge. The annealing temperature dependence of the specific contact resistivity of the Pt/Pd/Au contacts on *p*-AlGaN may be explained in terms of the reduction of bend banding (and hence the reduction of the Schottky barrier height) due to the shift of the surface Fermi level toward the valence-band edge, as noted from the shift of the Ga2*p* core level (Fig. 17). The shift of the surface Fermi level could be caused by an increase in carrier concentration near the GaN surface region. The AES results showed that annealing the contacts caused the occurrence of interfacial reactions between the metal scheme and AlGaN, resulting in the formation of Ptand Pd-related gallide phases. It was shown that Pd and Pt could react with GaN, and form Pd– and Pt–Ga-related compound phases. This is in good agreement with the results previously reported, showing that the Pt- and Pd gallides are particularly stable among the group-III metal gallides, since these metals are thermodynamically favored to react with gallium in GaN. The formation of either Pd- or Pt-gallides at the interface region indicates the out-diffusion of Ga from the AlGaN and hence the generation of Ga vacancies near the surface region of AlGaN. These Ga vacancies are known to serve as acceptors in *p*-AlGaN. The annealing-induced improvement of the *I–V* characteristics of the Pt/Pd/Au contacts could be attributed to the formation of gallides and as well as an increase in the contact areas between the metal scheme and AlGaN. A similar annealing-induced improvement of electrical properties was also observed in the Pt/Ni/Au and Pt/Au contacts on *p*-GaN.

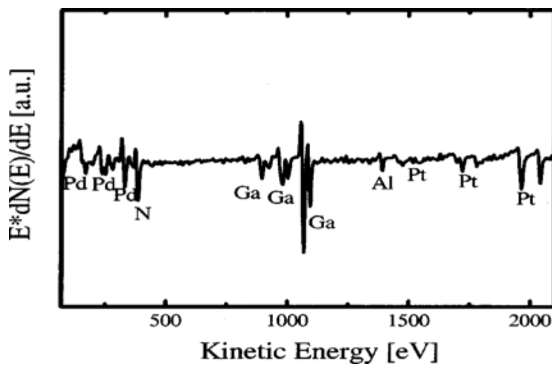

FIG. 16. Auger spectral data from the 600 °C annealed Pt/Pd/Au contacts.

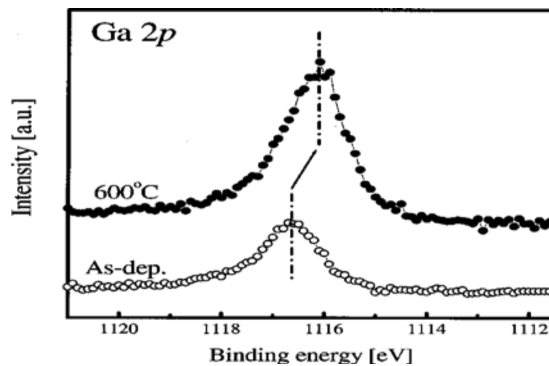

FIG. 17. The XPS Ga 2*p* core-level peaks before and after annealing at 600 °C.

3.B Low-resistance Pd/Ni/Au ohmic contacts to p-type GaN

Figure 18 shows I–V curves of Pd/Ni/Au contacts to p-GaN at various annealing temperatures. I–V curves were measured between the TLM pads with a gap spacing of 3 μm. The I–V curves show non-ohmic property for as-deposited samples, but they gradually proceeded toward ohmic characteristics as the alloying temperature was increased up to 500 ^{0}C. The specific contact resistivity was measured to be 2.4 x 10^{-5} Ω-cm^2 at this temperature. The improvement of ohmic property could be due to the high work function of the Pd and interfacial reactions taking place between the Pd, Ni, Au and GaN with their alloys extending into the GaN film. However, as the alloy temperature was increased to 600 ^{o}C, the I–V curve becomes nonlinear. Also, the resistivity and the morphology of the contacts deteriorated.

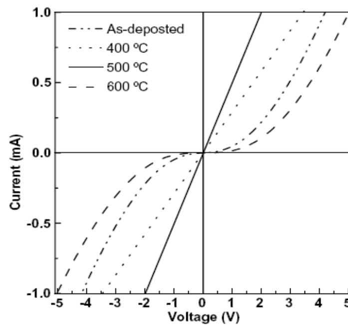

Fig. 18. I-V characteristics of Pd/Ni/Au contacts on p-Gan

Figure 19 shows AES depth profiles of Pd/Ni/Au contacts on p-GaN. For the as-deposited sample in Fig. 19 (a), no obvious evidence of inter-diffusion between the metal layers and the GaN exists. For the sample annealed at 500 ^{o}C, out-diffusion of Ni and Pd through Au layer is clearly observed in Fig. 19 (b). In the same figure, it is seen that there is also interdiffusion of Ni and Pd accompanied by penetration into the GaN film with possible formation of intermetallic compounds such as metallic gallides. Also, the oxygen content at the surface is high and its depth profile is similar to that of Ni. This points to NiO formation from Ni. Residual oxygen in the RTA chamber is the source of the reactant oxygen.

To identify any intermetallic compounds formed, we performed XPS analysis on alloyed contact metallizations. Many studies on XPS of Ni and Pd have explored the role of many-body effects in photoelectron spectra. Many-body effects lead to satellites in XPS spectra and small shifts between peaks. Satellites and peak asymmetry which arise in core-level XPS spectra provide information on the origin of metal alloys and show a strong dependence on the chemical environment. In addition, XPS depth profile provides a means to identify different chemical bonds at the interfaces of multilayered metals.

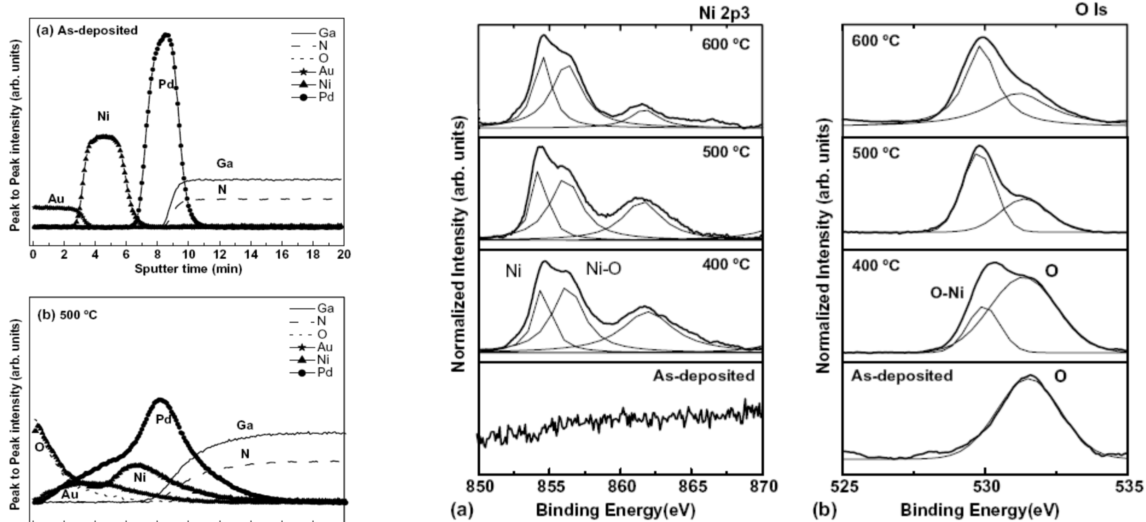

Fig. 19. The AES depth profiles od Pd/Ni/Au contacts on p-GaN films alloyed as-deposited (a) 500 ^{o}C annealing for 1 min (b).

Fig. 20. The Ni 2p3 (a), O 1s (b) XPS spectra of Pd/Ni/Au contacts on p-GaN films with various annealing temperatures.

Figures 20 (a) and (b) show the surface XPS spectra of Ni and O core-level at different annealing temperatures. As for the as-deposited sample, no Ni is observed, whereas out-diffusion of Ni is shown after annealing. It is clear that as the annealing temperature increases, satellites and peak asymmetry arise in the core-level XPS spectra. By a suitable combination of Gaussian functions, the spectral line shapes were fitted. When the Ni 2p3 spectra, as shown in Fig. 20 (a), was deconvoluted to three components after annealing corresponding to Ni–O bond and Ni–Pd–Au alloy, the spectra fitted well with experimental curves. The out-diffusion of Ni to the surface and uptake of O is believed to result from the annealing process. Ni seems to have prevented the out-diffusion of Pd through the formation of inter-metallic compounds with Pd and Au. Figure 20 (b) shows the spectra of O 1s core-level. As for as-deposited samples, the main line O 1s core-level is exhibited at 531.5 eV for different conditions. As annealing temperature increases, the main line reduces in intensity and the satellite peak of O–Ni bond at 530 eV which is associated with out-diffusion of Ni to the surface becomes stronger.

The depth profiles of XPS are shown in Fig. 21, where the relative intensities of Au, Ni, Pd, O, Ga, and N are plotted as a function of sputtering time. In the depth profiles

of the as-deposited sample, the interfaces between layers are evident, and no intermixing of species is believed to have occurred. Pd and Ni are not present at the surface where Au is mostly found. Also, as the sputter time increases, the Ni and Pd peak are sharp and there is minimal oxide formation. However, the depth profiles of the annealed sample indicate a considerable amount of intermixing, as no distinct interfaces can be determined between the individual layers. The binding energy of the Ni 2p3 peak indicates that the Ni on the surface of the annealed sample is in the form of NiO. The Ni signal remains intense as greater depths are probed into the GaN. It is evident that the Ni 2p3 core level peaks corresponding to Ni–Ga phases are present. Likewise, the O 1s peak also broadens at greater depths which show the presence of different forms of metallic oxides such as NiO. This result agrees with some reports on Ni penetration and reaction with a contamination/oxide layer on GaN; this was suggested as the basis for the achievement of low specific contact resistance on p-GaN. Also, Ni–O prevented Pd atoms from out-diffusing to the surface, as shown in Figs. 19 (b) and 21 (b).

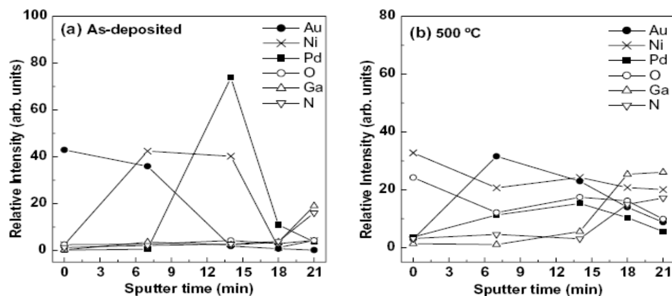

Fig.21. The XPS depth profiles of Pd/Ni/Au contacts on p-GaN film alloyed as-deposited (a), 500 ^{o}C annealing for 1 min (b)

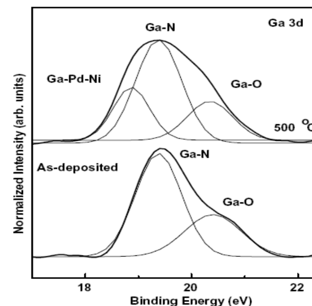

Fig. 22. The Ga 3d XPS spectra of Pd/Ni/Au contacts on p-GaN

Figure 22 shows the XPS spectra of Ga 3d core levels after sputtering for 18 min. As the annealing temperature increases, the binding energy of Ga 3d spectra reveals the presence of metallic-like Ga. With Gaussian fitting, three components such as Ga–Pd–Ni, Ga–N, and Ga–O bonds appeared in the sample annealed at 500 ^{o}C. This result suggests that Pd and Ni reacted with GaN, to form Pd- and Ni–Ga related compound phases. The production of Ga vacancy, acting as acceptors in the near-surface region of p-GaN plays a role in reducing contact resistivity. This is consistent with the results of previous studies, which indicated the formation of Ni–Ga and Pd–Ga phase such as Ga_4Ni_3, Ga_3Ni_2, and Ga_2Pd_5.

3.C Low-resistance Pd/Ir/Au ohmic contacts to p-type GaN

Figure 23 (a) shows the *I–V* characteristics measured between ohmic pads with a gap spacing of 5 µm as a function of annealing temperature. As-deposited contacts show slightly rectifying *I–V* characteristics, however, the *I–V* curves become almost linear at annealing temperatures between 400 and 500 °C. The best ohmic behavior was obtained at 400 °C with a contact resistivity as low as 2 x 10^{-5} Ω-cm^2. As the annealing temperature was increased to 600 °C, the contact property slightly degraded. The degradation is ascribed to the excessive interfacial reaction between metals (Pd, Ir, Au) and *p*-GaN. Figure 23 (b) shows the variation in the specific contact resistivity (ρ_c) and sheet resistance (R_S) of Pd/Au and Pd/Ir/Au contacts on GaN as a function of annealing temperature. Both samples exhibited their lowest contact resistances at 400 °C. When the samples were annealed at temperatures above 500 °C, the resistances slightly degraded. However, in the case of the Pd/Ir/Au scheme, the degradation in ρ_c is much lower than that of the Pd/Au scheme, which indicates that the Ir layer acted as an effective diffusion

barrier against the Au metal. Consequently, it is concluded that the Ir impeded Au diffusion toward the GaN surface.

Figure 24 shows AES depth profiles of Pd/Ir/Au contacts on *p*-type GaN for two different annealing temperatures. For the sample annealed at 400 °C shown in Fig. 24 (a), Pd reacted with GaN, and out-diffused to the Ir layer. In addition, small amounts of Pd out-diffused to the surface of the Au layer passing through the Ir layer. The out-diffused Pd atom passing through the Ir layer also induced the Ir in-diffusing to the surface of GaN due to Kirkendall effect. According to this effect, atomic diffusion occurs by a direct exchange mechanism or a ring mechanism in metallic crystals. The presence of Ir at the interface region was detected using XPS. For the samples annealed at 500 °C (not shown) and 600 °C, shown in Fig. 24 (b), Pd out-diffusion toward the surface of Au was more pronounced. Out-diffused Pd formed the Pd–Au alloy on the top of the contact. A small amount of Au diffused into the interface region through the Ir layer and reacted with the GaN, which may result in the formation of Au-related gallide. Although the formation of an Au–Ga alloy aids in reducing contact resistance in the ranges from 10^{-2} to 10^{4} Ωcm^2, the Au–gallide contributes to the degradation in low resistance contact because Au cannot form very low resistance ohmic contact to *p*-type GaN.

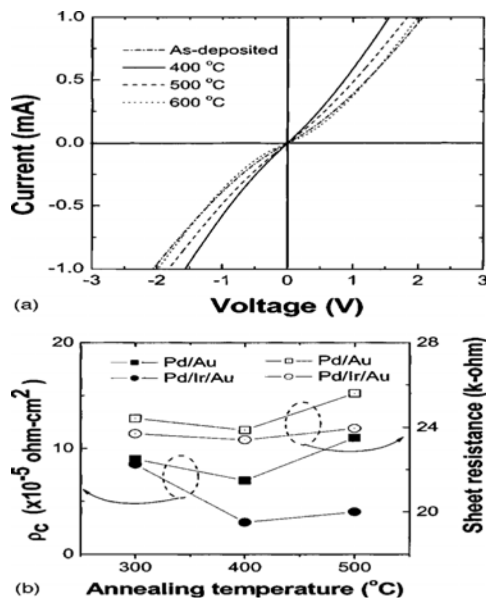

FIG. 23. *I–V* characteristics sad and the variations in the specific contact resistivity and sheet resistance sbd of Pd/ Ir/Au contacts on *p*-type GaN as a function of annealing temperature.

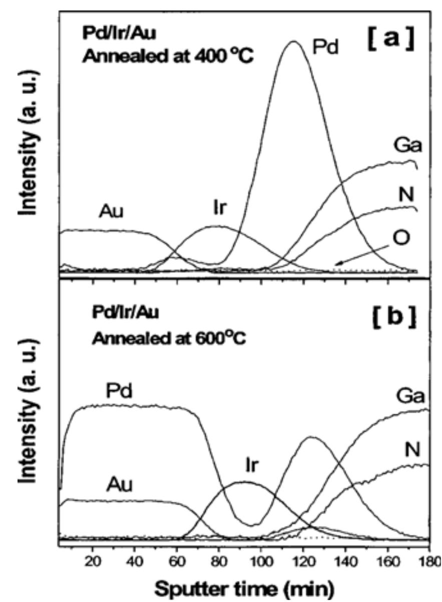

FIG. 24. AES depth profiles of: sad 400 °C and (b) 600 °C annealed Pd/ Ir/Au contacts on *p*-GaN

Detailed information about the interface region for the sample annealed at 400 °C was obtained by XPS. *In situ* sputter thinning was carried out with a low sputter rate of 1 nm/min. Figure 25 shows the XPS narrow scan spectra corresponding to the Ga 2*p* core level for different scan depths. The peak position of 1116.81 eV assigned to Ga in Ga–N bond at the surface region of GaN [curve (a)], shifted toward higher binding energy, as the sputtering depth approaches the bulk *p*-type GaN [curve (d)], where there are no Ga vacancies. The binding energy shift originated from the formation of Ga vacancies due to the out-diffusion of Ga atoms. The production of Ga vacancy in the near-surface region of GaN may lead to an increment in the net hole concentration below the contact. This results in the decrease of the depletion region width (*W*). Consequently, more carriers can tunnel through the reduced effective Schottky barrier. This is very consistent with the results previously reported by other authors. As the scanned surface approaches the bulk *p*-type GaN layer, the binding energy shifts toward higher energies by 0.36 eV in

comparison with the surface region of the GaN. This indicates that the concentration of Ga vacancies gradually decreased with the increase in the sputtered depth, and eventually became negligible at the bulk layer. There are also additional advantages of the annealing process: (i) increasing the contact area between the metal and GaN and (ii) enabling the diffusion of Pd into GaN where it can also act as an acceptor. These effects should help in reducing contact resistances. The effects of interfacial reactions between metals and *p*-type GaN are summarized in Fig. 26. The emission process change from thermionic emission (TE) to thermionic field emission (TFE) tends to occur at a carrier concentration in the 10^{17}–10^{18} cm^{-3} range at room temperature. Considering that the hole concentration of *p*-GaN used in this study was 5 x 10^{17} cm^{-3}, the carrier transport mechanism in the as-deposited contacts is dominated by the TFE process alongside a weak field emission (FE) process. After a moderate interfacial reaction, the depletion width was reduced due to the increased carrier concentration induced by the effects of Ga vacancies. This naturally resulted in a lowered SBH. The TE process becomes insignificant and FE starts to dominate, as the interfacial reactions increase the hole carrier concentration below the contact. It is required for LEDs to have a forward voltage of less than 3.5 V at 20 mA. This can only be achieved through the formation of excellent ohmic contacts to *p*-type GaN. Figure 27 shows typical *I–V* characteristics of blue GaN LEDs fabricated using our *p*-type contact materials. The LED heterostructures consisted of 0.2 µm Mg-doped, *p*-type GaN at the top with subsequent layers of 50 nm InGaN quantum well, 3 µm Si-doped *n*-type GaN on the GaN buffer layer grown on a sapphire substrate. Pd/Ir/Au was used as the *p*-contact metallization. It is shown that the forward voltage is 2.9 V at 20 mA. This is a low forward voltage when compared with those of other good LED devices. This work demonstrates that the Pd/ Ir/Au contact scheme should be very useful in fabricating high performance optoelectronic devices.

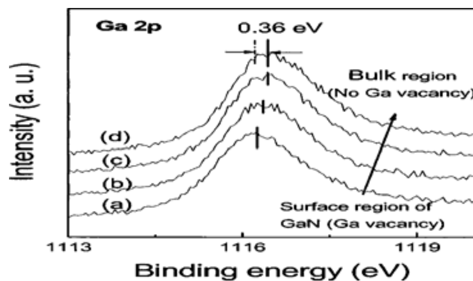

FIG. 25. XPS spectra of Ga 2*p* core level peaks for 400 °C annealed Pd/ Ir/Au contacts on *p*-GaN.

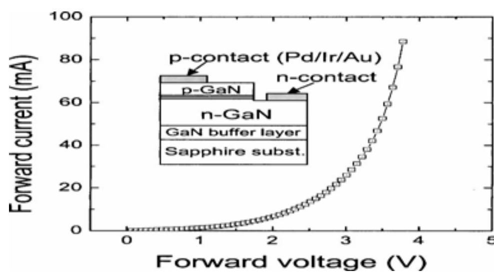

FIG. 27. Typical *I–V* characteristic of a blue LED device with Pd/ Ir/Au *p*-type ohmic contact.

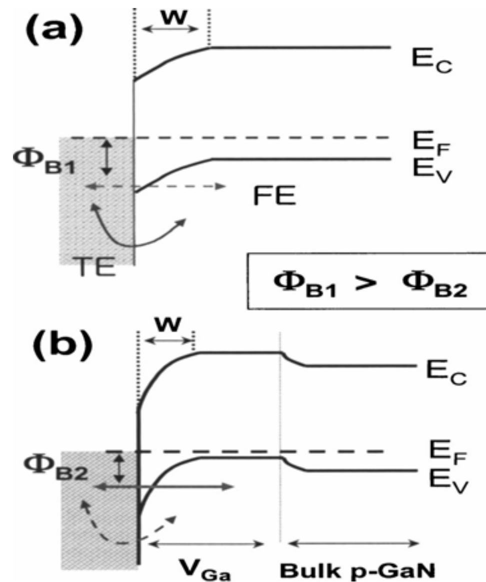

FIG. 26. Energy band diagram of Pd/ Ir/Au metallization *p*-type GaN junction: (a) before and (b) after annealing.

4. Summary and Conclusions

The efficacy of surface treatments on GaN and AlGaN to remove the surface native oxide has been investigated using XPS and AES measurements. NH_4OH, HCl, and BOE solutions were used to clean the GaN and AlGaN samples after $SiCl_4$ plasma

treatment, and of these, BOE was found to be the most effective treatment to remove oxide from the surface of the samples. Further, $SiCl_4$ plasma treatment coupled with wet etching on GaN resulted in a shift of Ga–N peaks to higher binding energies corresponding to a shift of the Fermi level toward the conduction band edge at the surface. This is believed to be caused by the creation of N vacancies on the surface due to $SiCl_4$ plasma treatment, which also corresponds to an increase in *n*-type dopant density on the surface. Similar result was obtained for AlGaN samples that were just plasma treated as well as those that were plasma treated and wet etched.

We have investigated the Pt/Pd/Au metallization scheme for the formation of ohmic contacts on moderately doped *p*-AlGaN:Mg (1.5 x 10^{17} cm^{-3}). It was shown that the electrical properties of the Pt/Pd/Au contacts improved with an increase in annealing temperature. In particular, the contact produced a very low specific contact resistivity, 3.1 x 10^{-4} Ω-cm^2, when annealed at 600 °C for 1 min.

We have investigated Pd/Ni/Au ohmic contacts to moderately doped p-GaN. Using 500 ^{o}C annealing in N_2 ambient, the specific contact resistance was found to be 2.4 x 10^{-5} Ω-cm^2. The formation of low specific contact resistance can be attributed to the high work function of Pd in contact with p-GaN and the effectiveness of the Pd layer in controlling the diffusion of Ni. AES and XPS data were presented to establish contact formation mechanism, which involved the formation of NiO along with Pd and Ni related gallide phases in the p-GaN surface region.

The Pd/Ir/Au contact scheme was applied to form low resistance ohmic contacts on *p*-GaN. The Ir layer between Pd and Au reduced the migration of Au toward the GaN, which kept ρ_c in the range of 10^{-5} Ω-cm^2 at moderately high annealing temperatures. Specifically, the Pd/Ir/Au contact exhibited a specific contact reisitivity (ρ_c) of 2 x 10^{-5} Ω-cm^2 at the annealing temperature of 400 °C. Ga vacancies acting as deep acceptors below contacts lowered the effective Schottky barrier heights and aided in reducing contact resistances.

Publications

1. Han-Ki Kim, Tae-Yeon Seong, Ilesanmi Adesida, Chak Wah Tang, and May Lau, “Low–resistance Pt/Pd/Au onmic contacts to p-type AlGaN,” Applied Physics Letters, vol 84, 1710 (2004).
2. Han-Ki Kim, I. Adesida, Tae-Yeon Seong, “Interfacial reaction effect on the ohmic properties of a Pt/Pd/Au contact on p-type GaN,” J. Vac. Sci. Technol. A 22, 1101 (2004).
3. H. K. Cho, T. Hossain, J. W. Bae, and I. Adesida, “Characterization of Pd/Ni/Au ohmic contacts on p-GaN,” Solid State Electronics 49, 774 (2005).
4. Deepak Selvanthan, Fitih M. Mohammed, Jeong-Oun Bae, Ilesanmi Adesida, and Katherine H. A. Bogart, “Investigation of surface treatment schemes on n-type GaN and AlGaN,” J. Vac. Sci. Technol B 23, 2538 (2005).
5. J. W. Bae, T. Hossain, I. Adesida, K. H. Bogart, D. Koleske, A.A. Allerman, and J. H. Jang, J. Vac. Sci. Technol B23, 1072 (2005).